Mechanism of ischemic brain injury repair by endothelial progenitor cell-derived exosomes

RUI HUANG*, TIANXIANG CHENG* and XIANLIANG LAI

Department of Neurosurgery, The Second Affiliated Hospital of Nanchang University, Nanchang, Jiangxi 330006, P.R. China

Received August 15, 2020; Accepted May 25, 2021

DOI: 10.3892/mmr.2022.12785

Abstract. Ischemic stroke is a refractory disease that seriously endangers human health and life. The main treatment aim of stroke is to alleviate brain injury. The present study aimed to investigate the effects and mechanisms of endothelial progenitor cell (EPC)-derived exosomes in repairing ischemic brain injury. Sprague-Dawley rat models of cerebral ischemia-reperfusion (IR) injury were established by middle cerebral artery occlusion. The IR model rats were then treated with PBS, EPC or exosomes; untreated and Sham rats were used as control. EPCs were obtained from tibias and femurs, and exosomes were isolated from the EPCs and characterized. To measure brain injury, 2,3,5-triphenyltetrazolium chloride staining was used to measure the infarct area, neurological deficit was scored, hematoxylin and eosin staining was used to examine pathological changes and TUNEL staining was used to quantify apoptosis. Immunofluorescence staining and reverse transcription-quantitative PCR were used to determine CD31 and VEGF protein and mRNA expressions, respectively, and western blot analysis was used out to measure the protein expression levels of Wnt3a, GSK-3β and phosphorylated (p)-GSK-3β. Compared with rats in the Control and Sham groups, in IR model rats the nerve fibers were slightly necrotic and swollen and the number of nerve cells was reduced. Following EPC treatment, the brain tissue exhibited mild liquefaction and degeneration in the small focus area with mild edema in the stroma. The numbers of nerve cells decreased, and the distribution of nerve cells was not very uniform; proliferation of glial cells was observed. Following treatment with exosomes, the distribution of nerve cells was more uniform with less degeneration and necrosis; the proliferation of glial cells was remarkable. Compared with the Control group, the infarct size, neurological defect score, percentage of apoptotic cells, expression of CD31, VEGF, Wnt3a, and p-GSK-3β were significantly higher in the IR model ($P<0.05$). After EPC and exosome treatments, the infarct size, neurological defect score, percentage of apoptotic cells, expression of Wnt3a, and p-GSK-3β were significantly reduced ($P<0.05$), whereas the mRNA and protein expression levels of CD31 and VEGF were significantly increased ($P<0.05$). Results from the present study demonstrated that EPC-derived exosomes may alleviate ischemic injury by inhibiting apoptosis and promoting angiogenesis. These findings suggested that exosomes may have a protective role for nerve cells and may be a potentially effective option for treating stroke. However, human clinical studies are needed to validate these findings from animals.

Introduction

Ischemic stroke is a refractory disease that can seriously harm human health and life. At present, the main treatment of stroke is to restore the blood supply to ischemic area as soon as possible to rescue dying neurons, glial cells and vascular endothelial cells (1). For acute ischemic stroke, the only effective way to restore blood supply is to use thrombolysis drugs and endovascular therapy within 3-4.5 h of the onset. This narrow treatment window and various complications, such as aneurysmal perforations induced by the microcatheter and thromboembolic events, also limit the use of endovascular therapy (2). How to effectively restore the blood supply in the ischemic brain tissue has become a key focus for stroke research (3). Stem cell-based therapy has been intensively applied to ischemic diseases. A number of previous studies have confirmed that the transplantation of stem cells can reduce tissue damage after ischemia and can promote the functional recovery of injured tissues (4-6). Endothelial progenitor cells (EPCs) have been shown to promote angiogenesis *in vitro* and *in vivo* (7,8). However, there are always risks involved in stem cell transplantation, such as vascular embolism caused by transplanted cells, genetic variation of cells cultured repeatedly *in vitro*, and the possibility of tumorigenesis and teratogenesis. Recently, the transport function and mechanism of extracellular microbubbles have attracted increased attention in various disciplines (9). In a broad sense, there

Correspondence to: Professor Xianliang Lai, Department of Neurosurgery, The Second Affiliated Hospital of Nanchang University, 1 Minde Road, Nanchang, Jiangxi 330006, P.R. China
E-mail: laixianliang123@126.com

*Contributed equally

Abbreviations: EPC, endothelial progenitor cell; IR, ischemia-reperfusion; SD, Sprague-Dawley rats; TEM, transmission electron microscopy; TTC, 2,3,5-triphenyltetrazolium chloride

Key words: endothelial progenitor cells, exosomes, ischemic brain injury, GSK-3β, phosphorlyated-GSK-3β, apoptosis, angiogenesis

are two extracellular vesicles: Exosomes and microvesicles. Microvesicles are ectosomes, or microparticles, a type of extracellular vesicle released from the cell membrane and are often uneven in size (diameter, ~1,000 nm). Exosomes are relatively uniform in size and form from the membrane of polyvesicles in the cell (10). Exosomes contain proteins, lipids, coding or non-coding RNAs and other bioactive substances similar to the source cells, such as cytokines and growth factors, and serve an important role in regulating the physiological functions of cells (11). A number of previous studies have investigated the repair of tissue damage by stem cell-derived exosomes. For example, the direct transplantation of exosomes secreted by stem cells into damaged tissues was reported to have a similar role in repairing tissue damage as that of transplanted stem cells (12). In addition, mesenchymal stem cell (MSC)-derived exosomes can promote the regeneration of nerval blood vessels to enhance the recovery of nerve function (13). In animal models of stoke and brain injury, MSC-derived exosomes were shown to enhance the coordination ability of movement by a horizontal transfer of mRNA, improving post-stroke neuroregeneration and rescuing cognitive impairments (14-16). In addition, EPC-derived exosomes have exhibited anti-apoptosis activity that promotes the proliferation and angiogenesis of endothelial cells (14) and the proliferation and differentiation of vascular endothelial cells (17). Sahoo *et al* (18) reported that the exosomes secreted by $CD34^+$ stem cells promote proliferation, migration and angiogenesis of endothelial cells *in vitro*. Therefore, stem cell-derived exosomes may also serve a role in promoting cell regeneration and repair, and they may be used to replace stem cells for therapy, thus avoiding the immune rejection that may result from stem cell transplantation.

In the present study, stem cell-derived exosomes were isolated and purified, and the effect and mechanism of repair on ischemia-reperfusion (IR) brain injury were investigated in model rats. The findings may provide a new insight on alleviating ischemic brain injury by EPCs and may facilitate the clinical translation of stem cell regenerative medicine.

Materials and methods

Animals. Male Sprague-Dawley (SD) rats (n=35; weight, 300 g; age, 9-10 weeks), were purchased from Slykingda Experimental Animal [Hunan, China; permit no. scxk (Xiang) 2016-0002]. Pregnant SD rats (n=3; weight 300 g; age, 9-10 weeks), were purchased from Tianqin Biotech [permit no. scxk (Xiang) 2016-0217]. All animal experiments and animal care were conducted in accordance with the criteria of the Laboratory Animals Welfare Act, the Guide for the Care and Use of Laboratory Animals provided by the Institutional Animal Care and Use Committee of Nanchang University. All experimental protocols for the use of animals were approved by the Animal Care and Use Committee of Nanchang University (Nanchang, China). All rats were housed under pathogen-free conditions at 30-70% humidity and 26˚C and had access to standard rodent food and water *ad libitum* and maintained under a 12-h light/dark cycle. Experiments were performed on rats between 7 and 10 weeks of age. Animals were euthanized after completion of the experiments and prior to tissue collection by CO_2 asphyxiation at a flow rate of 20% cage volume displacement/minute (5 l/min). Death after exposure to CO_2 was confirmed based on careful assessment of the rats for cardiac arrest.

Reagents and instruments. TUNEL assay kit (cat. no. C1088) was purchased from Beyotime Institute of Biotechnology. Rabbit antibodies against CD31 (cat. no. bs-20321R; 1:1,000) and GSK-3β (cat. no. bs-0028R; 1:1,000) were obtained from BIOSS; rabbit antibody against VEGF (cat. no. AF5109; 1:1,000) was obtained from Affinity; mouse monoclonal antibodies against β-actin (cat. no. TA-09; 1:2,000); HRP-conjugated goat anti-mouse IgG (H + L; cat. no. ZB-2305; 1:2,000) and HRP-conjugated goat anti-rabbit IgG (H + L; cat. no. ZB-2301; 1:2,000) were purchased from Zhongshan Golden Bridge Biotechnology Co., Ltd (OriGene Technologies, Inc.); rabbit polyclonal anti-phosphorylated (p)-GSK-3β (cat. no. AF2016; 1:500) was purchased from Affinity Biosciences, Ltd.; PVDF membrane (cat. no. IPVH00010) was purchased from MilliporeSigma; SuperSignal West Pico Chemiluminescent Substrate (cat. no. 34077) was obtained from Thermo Fisher Scientific, Inc.; Ultrasensitive Chemiluminescence Imaging system (ChemiDoc XRS$^+$) and CFX Connect Real-Time PCR Detection system were purchased from Bio-Rad Laboratories, Inc. Ultrapure RNA Extraction kit (cat. no. CW0581M) was purchased from CWBIO; HiScript II Q RT SuperMix for qPCR (cat. no. R223-01) was obtained from Vazyme; and Universal SYBR Green qPCR Master Mix was purchased from Applied Biosystems; Thermo Fisher Scientific, Inc.

EPC isolation. EPC isolation was performed as reported previously (19). Briefly, 3-day-old neonatal SD rats (n=3) from the pregnant females were sacrificed by decapitation and sterilized by soaking in 75% ethanol for 5 min. The tibia and femur were isolated, and the attached muscles were removed. The tibia and femur were washed with PBS and the bone marrow was washed into a Petri dish. The bone marrow was repeatedly pipetted to form a single cell suspension, which was then carefully added to the surface of 4 ml mixture of Ficoll, hydroxyethyl starch 550 and meglumine diatrizoate (20) and centrifuged at 500 x g for 20 min at 25-26˚C. The cells in the buffy coat fractions were collected, diluted with EBM-2 medium (cat. no. CC-3156; Lonza Group, Ltd.) and pelleted at 500 x g at 25-26˚C for 5 min. Cells were resuspended in EBM-2 medium and cultured in 2% CO_2 at 37˚C. The cells were then cultured in serum-free EBM-2 medium in a 2% CO_2 incubator at 37˚C for 48 h, collected and stored at -80˚C until exosome extraction. All operations were performed in laminar hoods to avoid microbial contamination.

Immunofluorescence assay. EPCs (10^4 cells/ml) were inoculated onto a microscope cover glass and cultured in EBM-2 medium in 2% CO_2 at 37˚C until cells reached 90% confluency. The slides were washed with PBS three times (3 min each), fixed at 25-26˚C with 4% paraformaldehyde for 15 min and permeated with 0.5% Triton X-100 (prepared in PBS) at room temperature for 20 min. The slides were then soaked in PBS for 5 min for three times (3 min each) at 25-26˚C. Cells were blocked with 5% BSA (CoWin Biosciences) at 37˚C for 30 min. Diluted primary rabbit anti-coagulation factor VIII antibody (cat. no. bs-2974R; BIOSS; 1:200) was added and the slides were incubated at 4˚C overnight. The slides were

subsequently incubated with Cy3-conjugated goat anti-rabbit IgG secondary antibody (1:200; cat no. S0011; Affinity Biosciences) at 37˚C for 30 min. The nuclei were stained with DAPI at 25-26˚C for 1 h and the slides were examined under a fluorescence microscope.

Exosome extraction. EPCs were rapidly thawed at 37˚C and the supernatant was centrifuged at 2,000 x g for 30 min at 4˚C. The supernatant was centrifuged again at 12,000 x g for 45 min at 4˚C to remove larger vesicles. The supernatant was then filtered through a membrane (0.45 μm pore size) and pelleted by centrifuging at 11,0000 x g for 70 min at 4˚C. The pellet was resuspended with 10 ml precooled 1X PBS. The exosome suspension was injected into a NanoFCM N30E nanoflow detector (Malvern Instruments, Ltd.) to determine the size distribution (diameter and number).

Transmission electron microscopy (TEM). EPCs were fixed in 2.5% glutaraldehyde at 25-26˚C for 1 h. After washing in pre-cooled PBS, the EPCs were dehydrated using ethanol and acetone, soaked in embedding solution overnight at room temperature and embedded in epoxy resin. Embedded cell blocks were cut into ultrathin sections (50-nm) and stained with 2% uranyl acetate for 30 min at 25-26˚C, and washed with water five times (10 sec each time). Then, the sections were stained with 1% lead citrate for 15 min at 25-26˚C and washed five times (10 sec each time) before TEM at 80 kV.

IR model and treatment. A classical suture method was used to establish IR models (21). Briefly, rats were anesthetized by intraperitoneal injection of ketamine 100 mg/kg (Shanghai Hengrui Pharmaceutical Co., Ltd.) and xylazine 10 mg/kg (Hubei Xinmingtai Chemical Co., Ltd.). A smooth incision was made along the middle line of the neck to separate bluntly the left sternocleidomastoid muscles and cervical muscles and to expose the right common carotid artery. The carotid artery was separated at the trident point to expose internal and external carotid arteries. The proximal ends of the right common carotid artery and external carotid artery were ligated, and the internal carotid artery was clamped with a vascular clip. A small incision was made on the right common carotid artery 1 cm away from the trigeminal nerve. A monofilament was introduced along the carotid artery into the brain to block the blood flow of the middle cerebral artery. After 2 h embolization, the thread was withdrawn. Nerve function defect was evaluated 24 h after reperfusion and scored as follows: i) 0, no symptoms of nerve injury; ii) 1, incomplete extension of the left front paw; iii) 2, circling left; iv) 3, falling to the left; and v) 4, loss of consciousness and unable to walk autonomously (22).

The 35 male SD rats were randomly divided into five groups (n=7 rats/group): i) untreated rats (control); ii) sham operation without plus inserted (sham); iii) IR model rats injected with 50 μl PBS (model); iv) model rats injected with 50 μl EPC cell suspensions at 6x10^6 cells/ml (model + EPC); v) and model rats injected with 50 μl exosome suspension at 0.6 μg/μl (model + exosome) once a day for 3 days. The dose of exosomes used was selected based on a previous study (23).

Three days before modelling, rats were anesthetized, fixed on a brain stereotaxic apparatus and a 1.5 cm longitudinal incision was made in the middle of the skin of the head. A skull drill was used to make a hole 0.22 mm posterior to and 10 mm to the right side of the bregma; care was taken to avoid damaging the dura. A total of 50 μl suspension (aforementioned) was administered using a microsyringe injector into the lateral ventricle below the surface of the skull. The needle was withdrawn slowly 5 min following injection, and the injection site was sterilized twice with iodophor and sutured. The mice were then placed on a thermal pad and reared in the cage when the animals were awake from the anesthesia.

2,3,5-triphenyltetrazolium chloride (TTC) staining. Rats were anesthetized as aforementioned and perfused with 20 ml PBS into the brain. The brain was dissected to isolate the cerebellum, brain stem and olfactory bulb. The brain tissues were frozen at -20˚C for 30 min and the cerebellum and olfactory bulb were removed. The remaining brain tissue was sectioned (2 mm thick) and stained in 2% TTC dye solution in the dark at 37˚C for 15 min; during this period, the sections were turned over every 5 min. The infarcted area was gray-white, and the non-infarcted area was dark red.

Hematoxylin and eosin (H&E) staining. H&E staining was conducted to examine the tissue damage as previously described (24). Briefly, the brain tissue was dehydrated in an ascending series of ethanol (70, 80, 90 and 100%) at 25-26˚C for 5 min at each concentration and cleared with xylene. Dehydrated tissue was embedded in paraffin, sectioned (4-μm thick), dewaxed with xylene and rehydrated in a series of ethanol (100, 90, 80, 70, 50, 30 and 0%) at 25-26˚C for 5 min at each concentration. The sections were stained with an aqueous hematoxylin solution at 25-26˚C for 3 min, differentiated with hydrochloric acid for 15 sec, briefly washed with tap water at 25-26˚C for 60 sec, and counterstained with eosin at 25-26˚C for 3 min. Sections were washed in distilled water, dehydrated and cleared as previously described, then the sections were sealed and examined under a CX41 light microscope (Olympus Corporation) at x200 magnification to observe pathological changes, including the number of nerve cells and glial cells.

TUNEL assay. A TUNEL assay was used to detect apoptotic cells in the brain tissues as described previously (25). Briefly, brain tissue sections (4-μm) were baked at 65˚C for 2 h, rehydrated in a descending ethanol series and treated with proteinase K (50 μg/ml) for 30 min at 37˚C. The sections were rinsed with PBS three times (5 min each) and incubated with TUNEL detection solution at 37˚C in the dark for 1 h, according to the supplier's protocols. The slide was then incubated with DAPI at room temperature in the dark for 3 min; the excess DAPI was rinsed away with PBS and the slide was blotted dry with absorbent paper. The slides were sealed with anti-fluorescence quenching solution and observed under a CX41 fluorescence microscope (Olympus Corporation) in 10 fields of view.

Reverse transcription-quantitative PCR (RT-qPCR). Total RNA was extracted from the brain tissues using an RNA Extraction kit (Takara Bio, Inc.) according to the manufacturer's instructions. RNA concentrations were quantified using

Table I. Primer sequences used for reverse transcription-quantitative PCR.

Gene	Primer sequence (5'-3')	Primer length, nt	Amplicon size, bp	Annealing temperature,˚C
VEGF	F: AATTGAGACCCTGGTGGACA	20	246	58.47
	R: CTATCTTTCTTTGGTCTGCATTCAC	25		
CD31	F: AGGTGACAGAAGGTGGGATT	20	299	56.85
	R: CTGGATTTGAAACTTGGGTG	20		
β-actin	F: GCCATGTACGTAGCCATCCA	20	375	59.53
	R: GAACCGCTCATTGCCGATAG	20		

F, forward; R, reverse; nt, nucleotide; bp, base pairs.

a Nanodrop spectrophotometer (NanoDrop Technologies; Thermo Fisher Scientific, Inc.) and subsequently reverse transcribed into cDNA using the High-Capacity cDNA Transcriptase Reverse kit (Applied Biosystems; Thermo Fisher Scientific, Inc.) according to manufacturer's protocol. qPCR was conducted using the Universal SYBR Green qPCR Master Mix (Applied Biosystems; Thermo Fisher Scientific, Inc.) on a CFX96 Real-Time PCR Detection System (Bio-Rad Laboratories, Inc.) using the primers listed in Table I. Relative mRNA expression levels were determined using the $2^{-\Delta\Delta Cq}$ method after normalization with β-actin as an internal reference (26). qPCR was carried out in a total volume of 15 μl containing 1 μl of diluted and pre-amplified cDNA, 10 μl Universal SYBR Green qPCR Master Mix and 1.5 μl of each forward and reverse primer. The thermocycling conditions were as follows: Initial denaturation at 95˚C for 10 min; followed by 40 cycles of 95˚C for 15 sec and 57˚C for 60 sec.

Immunofluorescence assays. Brain sections (4-μm) were fixed at 25-26˚C in 4% paraformaldehyde for 10-15 min and rinsed three times with PBS (3 min each). The cells were cleared with 0.5% Triton X-100 (in PBS) at room temperature for 20 min and washed with PBS three times (5 min each). After blocking with 5% BSA at 37˚C for 30 min, anti-CD31 antibody (1:1,000) was added and the plates were incubated overnight at 4˚C. The plates were then immersed in PBS three times (3 min each) and incubated with Cy3-conjugated goat anti-rabbit IgG (1:200; cat. no. CW0159S; CoWin Biosciences) at 25-26˚C for 1 h. Subsequently, the slides were incubated with an anti-VEGF antibody (1:1,000) at 25-26˚C for 30 min and then incubated with diluted Alexa Fluor 488-conjugated goat anti-rabbit IgG (1:200; cat. no. ZF-0511; Zhongshan Golden Bridge Biotechnology Co., Ltd; OriGene Technologies) at 37˚C for 45 min and counterstained with DAPI at 25-26˚C in the dark for 5 min. Images were captured using a fluorescence microscope (Olympus Corporation).

Western blotting. Brain tissues (0.2 g) were lysed with RIPA buffer (Beijing Solarbio Science & Technology Co., Ltd.) containing protease inhibitors cocktail and quantitated using a BCA kit (CoWin Biosciences) according to the manufacturer's instructions. After denaturing by boiling at 100˚C for 5 min, 50 μg protein was separated by 10% SDS-PAGE, transferred to PVDF membranes, blocked with 5% non-fat milk in 1X TBS-0.1% Tween-20 buffer for 4 h at room temperature and then detected by incubation with the following primary antibodies (at the aforementioned dilutions) at 4˚C overnight: Mouse monoclonal anti-β-actin, rabbit polyclonal anti-Wnt3α, rabbit polyclonal anti-Gsk-3β and rabbit polyclonal anti-p-Gsk-3β. Subsequently, the membranes were incubated with HRP-conjugated goat anti-mouse IgG or HRP-conjugated goat anti-rabbit IgG secondary antibodies (at the aforementioned dilutions) at 25-26˚C for 1 h. Protein bands were visualized using the SuperSignal West Pico Chemiluminescent Substrate (cat. no. 34077; Thermo Fisher Scientific, USA). Densitometric analysis was conducted using Quantity One software (version v4.6.6; Bio-Rad Laboratories, Inc.) using β-actin as the internal control.

Statistical analysis. Data are expressed as the mean ± standard error of the mean obtained from at least three independent experiments. Statistical comparisons between groups were assessed using one-way ANOVA with Tukey's post hoc tests. Ordinal data obtained for nerve defect scoring were analyzed using the Kruskal-Wallis test followed by Dunn's post hoc tests. Statistical analysis was performed using SPSS 21.0 software (IBM Corp.). $P<0.05$ was considered to indicate a statistically significant difference.

Results

Characterization of EPCs and exosomes. Immunofluorescence results demonstrated that isolated EPCs had red fluorescence with a wavelength 640 nm emitted from factor VIII (Fig. 1A). TEM and nanoflow measurements confirmed that the isolated exosomes exhibited the cup-like shape with double membranes (Fig. 1B) and were in the expected size range (30-299 nm), with the majority of exosomes being 60-80 nm in diameter (Fig. 2).

EPC and exosome treatment reduce infarcted area and nerve defects. Results from TTC staining revealed that the infarcted area increased significantly after IR modeling compared with the control and sham groups (Fig. 3A). EPC and exosome treatments significantly reduced the infarcted area compared with the untreated model group (Fig. 3A). Similarly, IR modelling significantly increased nerve defects compared with the control (Fig. 3B); the EPC and exosome treatments significantly reduced the defect score (Fig. 3B), and the improvement was more notable with exosome than with EPC ($P<0.05$; Fig. 3B).

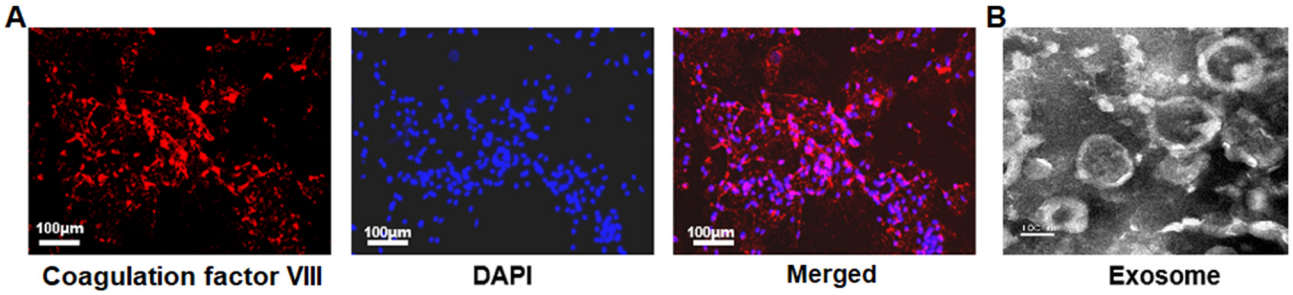

Figure 1. Characterization of EPCs and exosomes using immunofluorescence and TEM. (A) Immunofluorescence from EPCs. (B) TEM image demonstrating the morphology of exosomes. Scale bar, 100-μm. EPC, endothelial progenitor cell; TEM, transmission electron microscopy.

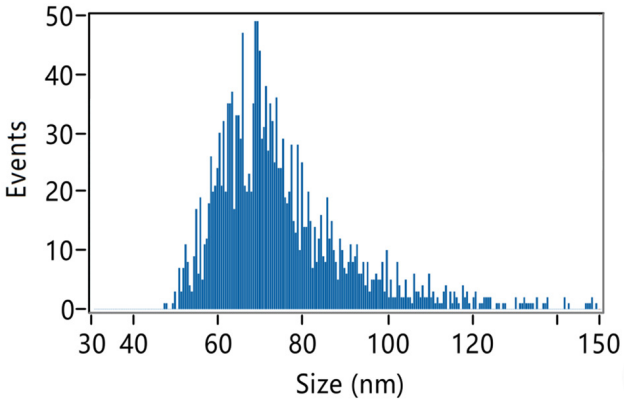

Figure 2. Size distribution of isolated exosomes under transmission electron microscopy.

EPC and exosome treatment reduce IR-induced degeneration and necrosis of nerve cells. H&E staining revealed that in control and sham rats, the boundary of the cortex and gray matter of the brain was clear without edema and necrosis; the nerve cells were arranged orderly and evenly, the cell membrane was intact and there was a clear nucleus and nucleolus (Fig. 4). In model group, the nerve fibers were slightly necrotic and swollen, the number of nerve cells was reduced and glial cells were proliferated. In the EPC-treated rats, the brain tissue showed mild liquefaction and degeneration, mild edema in the stroma and decreased number of nerve cells which were distributed less evenly; glial cells were proliferated. In the exosome-treated rats, the distribution of nerve cells was more uniform, the degeneration and necrosis of cells were less intensive, and the proliferation of glial cells was remarkable (Fig. 4).

EPC and exosome treatments reduce IR-induced apoptosis in nerve cells. The TUNEL assay results revealed that, compared with the control, the number of apoptotic cells was significantly increased after IR modelling (P<0.05; Fig. 5). Compared with the untreated model group, apoptosis was significantly decreased following EPC and exosome treatments (both P<0.05). Compared with EPC treatment, model rats treated with exosomes exhibited a significant reduction in apoptosis (P<0.05).

EPC and exosome treatments upregulate CD31 and VEGF expression. qPCR results revealed that the mRNA expression levels of CD31 and VEGF were significantly increased after IR modelling compared with the control group (P<0.05; Fig. 6); the expressions were further upregulated following EPC and exosome treatments compared with the untreated model group (both P<0.05). Similarly, immunofluorescence assay results demonstrated that the protein expression levels of CD31 and VEGF were significantly increased after IR modelling (P<0.05) compared with the control and sham groups, and they were further upregulated following EPC and exosome treatments (P<0.05), particularly with exosomes (P<0.05) (Fig. 7) compared with the model group.

EPC and exosome treatment downregulated Wnt3a and p-GSK-3 expression. Western blot analysis revealed that the protein expression levels of Wnt3a, GSK-3β and p-GSK-3β were significantly increased after IR modelling (P<0.05) compared with the control and sham groups, and were significantly downregulated in model rats treated with EPCs or exosomes compared with the control and sham groups; no significant difference in the ratio of p-GSK-3β to GSK-3β expression levels were detected (P>0.05) compared with the control and sham groups (Fig. 8). Exosome treatment resulted in a more marked downregulation compared with EPC treatment (P<0.05).

Discussion

Stroke is a common disease with high morbidity. It can be divided into hemorrhagic stroke and ischemic stroke, which is more common (27). To better understand ischemic cerebrovascular disease, it is very important to establish a relevant animal model for experimental investigation. In the present study, the classical suture method was used to occlude the middle cerebral artery to generate an IR model rat. The success of modelling was confirmed by the presence of infarcted area and reduced nerve defect score. Exosomes are extracellular vesicles with a diameter of 30-100 nm and a double layered membrane; they contain a variety of bioactive substances such as proteins, lipids and nucleic acids (28). Exosomes could stably exist in extracellular spaces and deliver proteins and RNA to the targeted cells to reprogram the recipient cells (29) and could play an important role in various physiological and pathological processes (30). In the present study, EPCs were isolated, and exosomes were extracted from the supernatant of EPCs. TEM revealed that the extraction of exosomes was successful, as the extracted exosomes exhibited the expected double membrane structure and size.

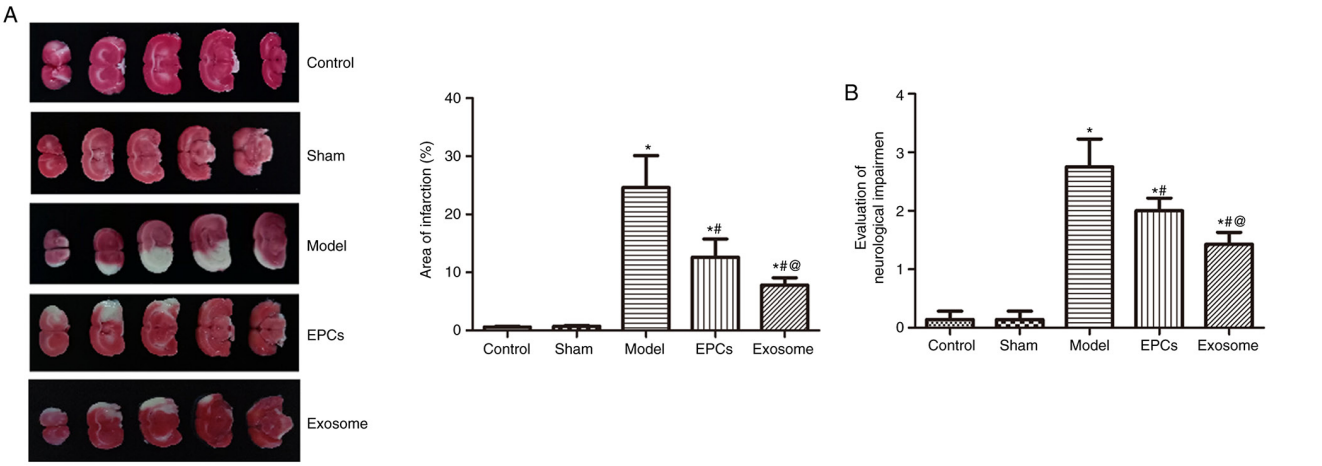

Figure 3. TTC staining and evaluation of nerve defect following EPC and exosome treatment. (A) Representative images of TTC staining and comparison of infarcted areas between groups. (B) Nerve defect score. *P<0.05 vs. control and sham, #P<0.05 vs. model and @P<0.05 vs. EPC. EPC, endothelial progenitor cell; TTC, 2,3,5-triphenyltetrazolium chloride.

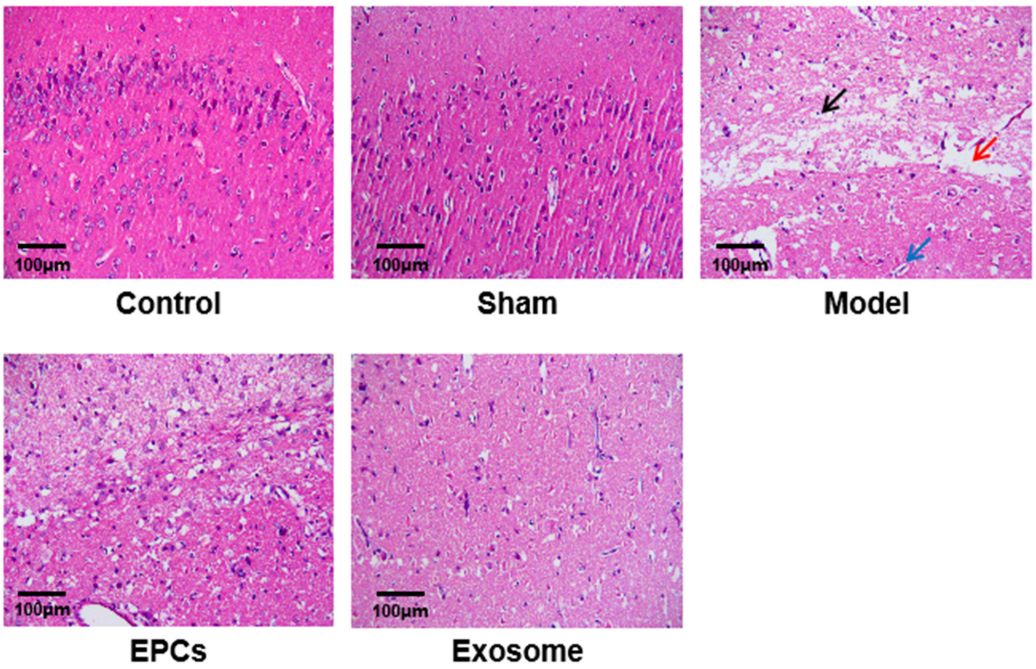

Figure 4. Hematoxylin and eosin staining of brain nerve cells following EPC and exosome treatment. Red arrows, edema; black arows, glial cells; and and blue arrows, nerve cells. EPC, endothelial progenitor cell.

A previous study reported that MSC-derived exosomes could improve the recovery of neural function by promoting neurovascular regeneration (13). Therapeutic effects of MSC-derived exosomes have been confirmed in animal models of stroke and brain injury, resulting in significant improvements in motor coordination and space learning ability (14-16). In addition, previous studies have demonstrated that EPC-secreted exosomes promote the proliferation and vessel formation of endothelial cells (14), as well as the proliferation and differentiation of vascular endothelial cells through anti-apoptotic effects (17). Bian *et al* (31) found that the exosomes from bone marrow MSCs promote angiogenesis in ischemic myocardium, reduce myocardial infarction area and improve cardiac function. Sahoo *et al* (18) also demonstrated that the exosomes secreted by $CD34^+$ stem cells promote the proliferation, migration and vessel formation of endothelial cells *in vitro*.

CD31 is present on the surface of platelets, neutrophils, monocytes and certain types of T cells, as well as in the junctions between endothelial cells. It may be involved in leukocyte migration, angiogenesis and integrin activation (32,33). The expression of CD31 is significantly upregulated after cerebral ischemia and is further increased after treatment with exosomes (19). The angiogenesis of endothelial cells is regulated by a number of angiogenic genes, including VEGF (17,34). VEGF is an important angiogenic factor that mediates the proliferation and migration of endothelial cells and maintains the survival of vascular endothelium after binding with kinase insert domain receptor in vascular endothelial cells (35).

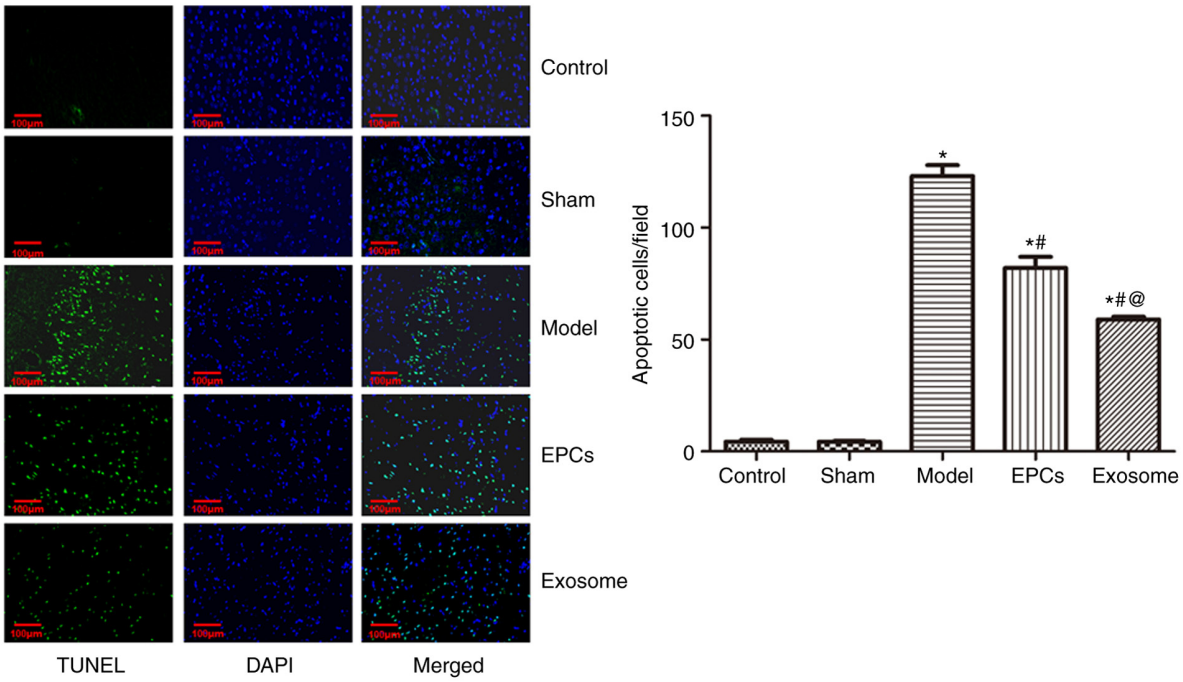

Figure 5. TUNEL assays of brain nerve cells following in EPC and exosome treatment. Representative images of TUNEL staining (right) were used to count and compare the number of apoptotic cells (left). *P<0.05 vs. control and sham, #P<0.05 vs. model and @P<0.05 vs. EPC. EPC, endothelial progenitor cell.

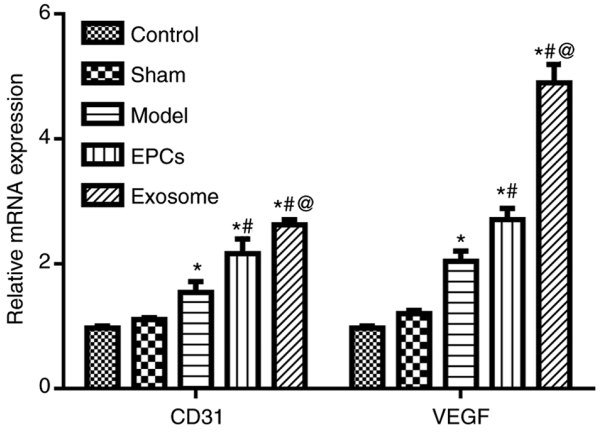

Figure 6. Reverse transcription-quantitative PCR detection of the mRNA expression levels of CD31 and VEGF in brain nerve cells following in EPC and exosome treatment. *P<0.05 vs. control and sham, #P<0.05 vs. model and @P<0.05 vs. EPC. EPC, endothelial progenitor cell.

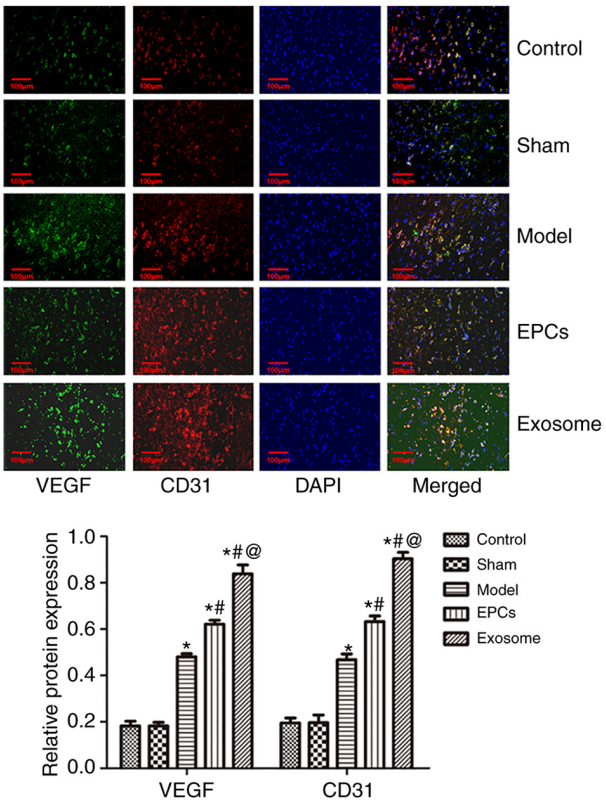

Figure 7. Immunofluorescence assay of CD31 and VEGF protein expression levels in brain nerve cells following EPC and exosome treatment. *P<0.05 vs. control and sham, #P<0.05 vs. model and @P<0.05 vs. EPC. EPC, endothelial progenitor cell.

EPCs usually exist in bone marrow. When peripheral tissues are damaged by ischemia and hypoxia, VEGF and other substances are produced in the injured tissues to mobilize and recruit EPCs to the ischemic and hypoxic tissues, where the EPCs are integrated into the blood vessels to promote the extension of the original blood vessels and to provide materials for angiogenesis by secreting a variety of angiogenesis-related substances, such as VEGF (36,37). As a consequence, angiogenesis and functional recovery of ischemic tissues are facilitated (38,39). Data from the present study demonstrated that the expression of CD31 and VEGF increased significantly after cerebral ischemia and further increased after EPC or exosome treatment, suggesting that one of the mechanisms underlying exosome-mediated angiogenesis is to upregulate the expression of angiogenesis related-genes and proteins in the endothelial cells, thus promoting angiogenesis.

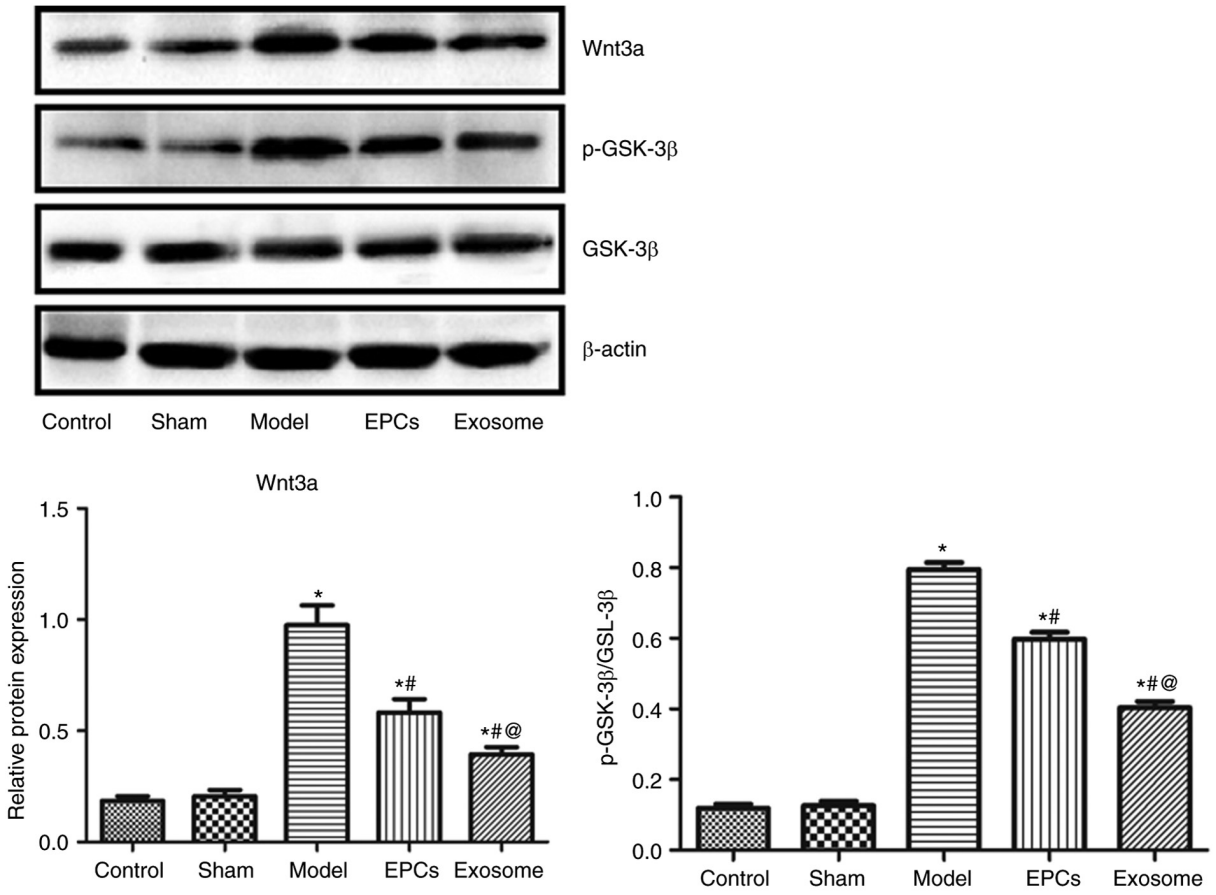

Figure 8. Western blot analysis of Wnt3a, GSK-3β and p-GSK-3β protein expression levels in brain nerve cells following EPC and exosome treatment. *P<0.05 vs. control and sham, #P<0.05 vs. model and @P<0.05 vs. EPC. EPC, endothelial progenitor cell; p, phosphorylated.

The Wnt signaling pathway is a well-known intracellular signaling pathway, which is highly conserved evolutionally. This pathway is involved in the proliferation, differentiation and axon formation of neural stem cells, and serves an important role in the formation and maintenance of the blood-brain barrier, cerebral vascular regeneration and remodeling (40). A previous study demonstrated that Wnt signaling pathway serves an important role in injury repair and neurovascular remodeling following ischemic stroke (41). It has been reported that treatment with the GSK-3β inhibitor TWS119 reduces neurological deficit score and increases brain edema, infarct volume and blood-brain barrier damage as a result of Wnt signaling pathway activation (42). A previous study also found that the Wnt signaling pathway in rats is activated when ischemic stroke occurs (35). Activated Wnt signaling pathway is accompanied with increased GSK-β phosphorylation (43,44). The present study also revealed that the levels of Wnt3 and p-GSK-β were increased after cerebral ischemia. The levels of Wnt3 and p-GSK-β were downregulated in model rats treated with EPCs or exosomes, suggesting that EPC derived-exosomes may be neuroprotective by inhibiting the expression of Wnt3 and phosphorylation of GSK-β.

There are limitations to the present study. First, the therapeutic effects of EPC exosomes on ischemic stroke were investigated *in vivo*, but not *in vitro*. The dose of EPC exosomes has not been optimized since only a single dose was used in this study. Although EPC-derived exosomes serve neuroprotective effects by inhibiting Wnt3 expression and GSK-β phosphorylation, as well as promote angiogenesis by upregulating the expression of angiogenesis-related genes and proteins in endothelial cells (42), there is a lack of investigations on the mechanisms underlying its regulation. Moreover, microRNAs (miRNAs/miRs) in exosomes serve an important role in injury repair. For example, M1 macrophages are known to promote inflammation; on other hand, exosomes secreted from adipose-derived stem cells rich in miR-30d-5p inhibited autophagy-mediated polarization of microglia to M1, thereby preventing brain damage caused by inflammation (45). Therefore, it is worthy to screen miRNAs in EPC-derived exosomes and to investigate their possible mechanisms. Since this study was focused on the Wnt/GSK-β pathway, the downstream effectors have not been investigated. Therefore, as these genes and proteins, such as downstream effectors, are likely to play role in the observed therapeutic effect, they should be investigated to further elucidate the therapeutic mechanisms and potential in attenuating IR-induced damage. For example, Petherick *et al* (46) found that the accumulation of β-catenin inhibited the p62/SQSTM1 promoter, leading to autophagy inhibition, and Chen *et al* (47) reported that TNFα inhibits osteogenic differentiation by inhibiting the Wnt/β-catenin pathway, and subsequently inhibits autophagy. The use of autophagy inducers restores the TNFα-mediated differentiation process and positively regulates the Wnt/β-catenin pathway.

In conclusion, the present study demonstrated that EPC-derived exosomes reduced apoptosis and promoted angiogenesis, and may serve a protective role to nerve cells with IR-induced damage. Therefore, exosomes may be considered as a potential therapeutic agent for stroke, although clinical studies in humans are required to validate these findings. Compared with other therapeutics, such as intravenous thrombolysis and endovascular mechanical thrombectomy, exosomes may target the recipient cells selectively due to expression of tissue-specific antigens on the surface of exosome.

Acknowledgements

Not applicable.

Funding

This work was funded by Jiangxi Provincial Science and Technology Department (grant no. 20161BBH80075).

Availability of data and materials

The datasets used and/or analyzed during the current study are available from the corresponding author on reasonable request.

Authors' contributions

RH, TC and XL designed the study. RH and TC collected the data and performed the analyses. RH, TC and XL drafted the manuscript. RH and XL confirm the authenticity of all the raw data. All authors read and approved the final manuscript.

Ethics approval and consent to participate

All animal experiments and animal care were conducted in accordance with the criteria of the Laboratory Animals Welfare Act, the Guide for the Care and Use of Laboratory Animals provided by the Institutional Animal Care and Use Committee Nanchang University (Nanchang, China). All experimental protocols for the use of animals were approved by the Animal Care and Use Committee Nanchang University (Nanchang, China).

Patient consent for publication

Not applicable.

Competing interests

The authors declare that they have no competing interests.

References

1. Jena I, Nayak SR, Behera S, Singh B, Ray S, Jena D, Singh S and Sahoo SK: Evaluation of ischemia-modified albumin, oxidative stress, and antioxidant status in acute ischemic stroke patients. J Nat Sci Biol Med 8: 110-113, 2017.
2. Yoshimura S, Sakai N, Uchida K, Yamagami H, Ezura M, Okada Y, Kitagawa K, Kimura K, Sasaki M, Tanahashi N, *et al*: Endovascular therapy in ischemic stroke with acute large-vessel occlusion: Recovery by endovascular salvage for cerebral ultra-acute embolism Japan Registry 2. J Am Heart Assoc 7: e008796, 2018.
3. Moussouttas M and Papamitsakis NIH: Critique on the use of early short-term dual antiplatelet therapy following minor acute cerebral ischemic events. Cerebrovasc Dis 49: 237-243, 2020.
4. Abdelwahid E, Siminiak T, Guarita-Souza LC, Teixeira de Carvalho KA, Gallo P, Shim W and Condorelli G: Stem cell therapy in heart diseases: A review of selected new perspectives, practical considerations and clinical applications. Curr Cardiol Rev 7: 201-212, 2011.
5. Gutierrez-Fernandez M, Rodriguez-Frutos B, Ramos-Cejudo J, Otero-Ortega L, Fuentes B and Diez-Tejedor E: Stem cells for brain repair and recovery after stroke. Expert Opin Biol Ther 13: 1479-1483, 2013.
6. Lee EJ, Park HW, Jeon HJ, Kim HS and Chang MS: Potentiated therapeutic angiogenesis by primed human mesenchymal stem cells in a mouse model of hindlimb ischemia. Regen Med 8: 283-293, 2013.
7. Wu Y, Ip JE, Huang J, Zhang L, Matsushita K, Liew CC, Pratt RE and Dzau VJ: Essential role of ICAM-1/CD18 in mediating EPC recruitment, angiogenesis, and repair to the infarcted myocardium. Circ Res 99: 315-322, 2006.
8. Asahara T, Masuda H, Takahashi T, Kalka C, Pastore C, Silver M, Kearne M, Magner M and Isner JM: Bone marrow origin of endothelial progenitor cells responsible for postnatal vasculogenesis in physiological and pathological neovascularization. Circ Res 85: 221-228, 1999.
9. Gong XH, Liu H, Wang SJ, Liang SW and Wang GG: Exosomes derived from SDF1-overexpressing mesenchymal stem cells inhibit ischemic myocardial cell apoptosis and promote cardiac endothelial microvascular regeneration in mice with myocardial infarction. J Cell Physiol 234: 13878-13893, 2019.
10. Xue M, Chen W, Xiang A, Wang R, Chen H, Pan J, Pang H, An H, Wang X, Hou H and Li X: Hypoxic exosomes facilitate bladder tumor growth and development through transferring long non-coding RNA-UCA1. Mol Cancer 16: 143, 2017.
11. Tian T, Zhang HX, He CP, Fan S, Zhu YL, Qi C, Huang NP, Xiao ZD, Lu ZH, Tannous BA and Gao J: Surface functionalized exosomes as targeted drug delivery vehicles for cerebral ischemia therapy. Biomaterials 150: 137-149, 2018.
12. Qu Y, Zhang Q, Cai X, Li F, Ma Z, Xu M and Lu L: Exosomes derived from miR-181-5p-modified adipose-derived mesenchymal stem cells prevent liver fibrosis via autophagy activation. J Cell Mol Med 21: 2491-2502, 2017.
13. Xin H, Li Y, Cui Y, Yang JJ, Zhang ZG and Chopp M: Systemic administration of exosomes released from mesenchymal stromal cells promote functional recovery and neurovascular plasticity after stroke in rats. J Cereb Blood Flow Metab 33: 1711-1715, 2013.
14. Deregibus MC, Cantaluppi V, Calogero R, Lo Iacono M, Tetta C, Biancone L, Bruno S, Bussolati B and Camussi G: Endothelial progenitor cell derived microvesicles activate an angiogenic program in endothelial cells by a horizontal transfer of mRNA. Blood 110: 2440-2448, 2007.
15. Kim DK, Nishida H, An SY, Shetty AK, Bartosh TJ and Prockop DJ: Chromatographically isolated CD63+CD81+ extracellular vesicles from mesenchymal stromal cells rescue cognitive impairments after TBI. Proc Natl Acad Sci USA 113: 170-175, 2016.
16. Doeppner TR, Herz J, Gorgens A, Schlechter J, Ludwig AK, Radtke S, de Miroschedji K, Horn PA, Giebel B and Hermann DM: Extracellular vesicles improve post-stroke neuroregeneration and prevent postischemic immunosuppression. Stem Cells Transl Med 4: 1131-1143, 2015.
17. Cantaluppi V, Biancone L, Figliolini F, Beltramo S, Medica D, Deregibus MC, Galimi F, Romagnoli R, Salizzoni M, Tetta C, *et al*: Microvesicles derived from endothelial progenitor cells enhance neoangiogenesis of human pancreatic islets. Cell Transplant 21: 1305-1320, 2012.
18. Sahoo S, Klychko E, Thorne T, Misener S, Schultz KM, Millay M, Ito A, Liu T, Kamide C, Agrawal H, *et al*: Exosomes from human CD34(+) stem cells mediate their proangiogenic paracrine activity. Circ Res 109: 724-728, 2011.
19. Roy J: Primary microglia isolation from mixed cell cultures of neonatal mouse brain tissue. Brain Res 1689: 21-29, 2018.
20. Xu L, Li X, Zhang E, Liang H, Li W, Wang S, Song S and Ji A: The effect of leech extracts on endothelial cell coagulation-related factors and endothelial dysfuction-related molecules. Clin Exp Hypertens 41: 220-230, 2019.
21. Zhao J, Zhao Y, Zheng W, Lu Y, Feng G and Yu S: Neuroprotective effect of curcumin on transient focal cerebral ischemia in rats. Brain Res 1229: 224-232, 2008.

22. Wei EQ, Zhu CY, Xu QQ, Yu YP, Zhu YF and Zheng MZ: An improved quantitative method for evaluating neurological deficits in mice with focal cerebral ischemia. Sheng Li Xue Bao 55: 742-747, 2003 (In Chinese).
23. AbuBakr N, Haggag T, Sabry D and Salem ZA: Functional and histological evaluation of bone marrow stem cell-derived exosomes therapy on the submandibular salivary gland of diabetic Albino rats through TGFβ/Smad3 signaling pathway. Heliyon 6: e03789, 2020.
24. Fischer AH, Jacobson KA, Rose J and Zeller R: Hematoxylin and eosin staining of tissue and cell sections. CSH Protoc 2008: pdb prot4986, 2008.
25. Kyrylkova K, Kyryachenko S, Leid M and Kioussi C: Detection of apoptosis by TUNEL assay. Methods Mol Biol 887: 41-47, 2012.
26. Livak KJ and Schmittgen TD: Analysis of relative gene expression data using real-time quantitative PCR and the 2(-Delta Delta C(T)) Method. Methods 25: 402-408, 2001.
27. Esenwa C and Gutierrez J: Secondary stroke prevention: Challenges and solutions. Vasc Health Risk Manag 11: 437-450, 2015.
28. Pegtel DM and Gould SJ: Exosomes. Annu Rev Biochem 88: 487-514, 2019.
29. Chen L, Guo P, He Y, Chen Z, Chen L, Luo Y, Qi L, Liu Y, Wu Q, Cui Y, *et al*: HCC-derived exosomes elicit HCC progression and recurrence by epithelial-mesenchymal transition through MAPK/ERK signalling pathway. Cell Death Dis 9: 513, 2018.
30. Miranda AM, Lasiecka ZM, Xu Y, Neufeld J, Shahriar S, Simoes S, Chan RB, Oliveira TG, Small SA and Di Paolo G: Neuronal lysosomal dysfunction releases exosomes harboring APP C-terminal fragments and unique lipid signatures. Nat Commun 9: 291, 2018.
31. Bian S, Zhang L, Duan L, Wang X, Min Y and Yu H: Extracellular vesicles derived from human bone marrow mesenchymal stem cells promote angiogenesis in a rat myocardial infarction model. J Mol Med (Berl) 92: 387-397, 2014.
32. Figueiredo CC, Pereira NB, Pereira LX, Oliveira LAM, Campos PP, Andrade SP and Moro L: Double immunofluorescence labeling for CD31 and CD105 as a marker for polyether polyurethane-induced angiogenesis in mice. Histol Histopathol 34: 257-264, 2019.
33. Shih YT, Wang MC, Yang TL, Zhou J, Lee DY, Lee PL, Yet SF and Chiu JJ: β(2)-Integrin and Notch-1 differentially regulate CD34(+)CD31(+) cell plasticity in vascular niches. Cardiovasc Res 96: 296-307, 2012.
34. Shima DT, Gougos A, Miller JW, Tolentino M, Robinson G, Adamis AP and D'Amore PA: Cloning and mRNA expression of vascular endothelial growth factor in ischemic retinas of Macaca fascicularis. Invest Ophthalmol Vis Sci 37: 1334-1340, 1996.
35. Melincovici CS, Bosca AB, Susman S, Mărginean M, Mihu C, Istrate M, Moldovan IM, Roman AL and Mihu CM: Vascular endothelial growth factor (VEGF)-key factor in normal and pathological angiogenesis. Rom J Morphol Embryol 59: 455-467, 2018.
36. Kamel NM, Abd El Fattah MA, El-Abhar HS and Abdallah DM: Novel repair mechanisms in a renal ischaemia/reperfusion model: Subsequent saxagliptin treatment modulates the pro-angiogenic GLP-1/cAMP/VEGF, ANP/eNOS/NO, SDF-1α/CXCR4, and Kim-1/STAT3/HIF-1α/VEGF/eNOS pathways. Eur J Pharmacol 861: 172620, 2019.
37. Li L, Liu H, Xu C, Deng M, Song M, Yu X, Xu S and Zhao X: VEGF promotes endothelial progenitor cell differentiation and vascular repair through connexin 43. Stem Cell Res Ther 8: 237, 2017.
38. Kutikhin AG, Sinitsky MY, Yuzhalin AE and Velikanova EA: Shear stress: An essential driver of endothelial progenitor cells. J Mol Cell Cardiol 118: 46-69, 2018.
39. Kumar VV, Heller M, Gotz H, Schiegnitz E, Al-Nawas B and Kammerer PW: Comparison of growth & function of endothelial progenitor cells cultured on deproteinized bovine bone modified with covalently bound fibronectin and bound vascular endothelial growth factor. Clin Oral Implants Res 28: 543-550, 2017.
40. Kahn M: Wnt signaling in stem cells and cancer stem cells: A tale of two coactivators. Prog Mol Biol Transl Sci 153: 209-244, 2018.
41. Oh SH, Kim HN, Park HJ, Shin JY and Lee PH: Mesenchymal stem cells increase hippocampal neurogenesis and neuronal differentiation by enhancing the Wnt signaling pathway in an Alzheimer's disease model. Cell Transplant 24: 1097-1109, 2015.
42. Wang W, Li M, Wang Y, Li Q, Deng G, Wan J, Yang Q, Chen Q and Wang J: GSK-3β inhibitor TWS119 attenuates rtPA-induced hemorrhagic transformation and activates the Wnt/β-catenin signaling pathway after acute ischemic stroke in rats. Mol Neurobiol 53: 7028-7036, 2016.
43. Chen S, Sun YY, Zhang ZX, Li YH, Xu ZM and Fu WN: Transcriptional suppression of microRNA-27a contributes to laryngeal cancer differentiation via GSK-3β-involved Wnt/β-catenin pathway. Oncotarget 8: 14708-14718, 2017.
44. Zhang X, Liu Y, Shao R and Li W: Cdc42-interacting protein 4 silencing relieves pulmonary fibrosis in STZ-induced diabetic mice via the Wnt/GSK-3β/β-catenin pathway. Exp Cell Res 359: 284-290, 2017.
45. Jiang M, Wang H, Jin M, Yang X, Ji H, Jiang Y, Zhang H, Wu F, Wu G, Lai X, *et al*: Exosomes from MiR-30d-5p-ADSCs reverse acute ischemic stroke-induced, autophagy-mediated brain injury by promoting M2 microglial/macrophage polarization. Cell Physiol Biochem 47: 864-878, 2018.
46. Petherick KJ, Williams AC, Lane JD, Ordóñez-Morán P, Huelsken J, Collard TJ, Smartt HJ, Batson J, Malik K, Paraskeva C and Greenhough A: Autolysosomal β-catenin degradation regulates Wnt-autophagy-p62 crosstalk. EMBO J 32: 1903-1916, 2013.
47. Chen L, Yang Y, Bao J, Wang Z, Xia M, Dai A, Tan J, Zhou L, Wu Y and Sun W: Autophagy negative-regulating Wnt signaling enhanced inflammatory osteoclastogenesis from Pre-OCs in vitro. Biomed Pharmacother 126: 110093, 2020.